Research Article | Vol. 8, No. 11 | 1 Nov 2018 | OPTICAL MATERIALS EXPRESS 3424
Optical Materials EXPRESS

# Nonlinear properties of the depressed cladding single mode $TeO_2$-$WO_3$-$Bi_2O_3$ channel waveguide fabricated by direct laser writing

A. G. OKHRIMCHUK,[1,2,*] YU. P. YATSENKO,[2] M. P. SMAYEV,[1,3] V. V. KOLTASHEV,[2] AND V. V. DOROFEEV[4]

[1]*Mendeleev University of Chemical Technology of Russia, 9 Miusskaya Square, Moscow 125047, Russia*
[2]*Fiber Optics Research Center of Russian Academy of Sciences, 38 Vavilova Street, Moscow 119333, Russia*
[3]*Lebedev Physical Institute of Russian Academy of Sciences, 53 Leninsky Prospect, Moscow 119991, Russia*
[4]*G.G. Devyatykh Institute of Chemistry of High-Purity Substances of Russian Academy of Sciences, 49 Tropinina St., Nizhny Novgorod 603951, Russia*
[*]*a.okhrim@yandex.ru*

**Abstract:** A large mode area depressed cladding waveguide was inscribed by a femtosecond laser beam in bulk of high purity $70TeO_2$-$22WO_3$-$8Bi_2O_3$ glass. Non-linear propagation of femtosecond pulses in the single mode waveguide with mode field diameter of 12 μm was investigated under input at 1030 nm wavelength. The highest peak value of a Raman-gain coefficient of all the tellurite glasses was measured ($1.2x10^{-9}$ cm/W). The dispersion of the refractive index was obtained in the range of 1170-2300 nm. Spectrum broadening of up to 160 nm at the −10 dB level was observed under input pulse energy as low as 84 nJ in a 14 mm long waveguide. The spectrum broadening was numerically simulated, and it was found that both the Kerr and the Raman nonlinearities result to comparable contributions to the spectrum transformation.



## 1. Introduction

An imminent need to avoid the information capacity crunch ultimately requires faster alternatives to semiconductor electronics. A rapidly developing nonlinear integrated photonics is widely recognized as one of the most promising alternatives [1]. Materials and manufacturing methods for photonic chips are currently under development. A conventional approach based on a conversion of the planar (2D) lithography initially developed for silicon microelectronics does not appear an optimal solution, because it cannot exploit the wave nature of photon, and new opportunities should be explored towards 3D architecture of optical circuits. The direct laser writing with femtosecond pulses is widely recognized as a straightforward and relatively simple technology for manufacturing of three-dimensional photonic circuits in the bulk of glasses and crystals [2]. Materials with high Kerr nonlinearity $\chi(3)$ play crucial role in nonlinear photonics. Chalcogenide and tellurite glasses are of great interest in this respect. In particular, the chalcogenide glasses have a great advantage of huge optical nonlinearity with $\chi(3)$ of two to three orders of magnitude exceeding that of silica glasses, however they generally suffer from low mechanical strength, impurity absorptions at specific wavelengths and low glass transition temperatures (< 250 °C). Compared with them, tellurite glasses have lower toxicity, better chemical and thermal stability, corrosion resistance, moderate glass transition temperature (280-440 °C, depending on the added modifying agents). A tellurite glass possesses high optical nonlinearity so that $\chi(3)$ is about 20-30 times higher than for silica glasses, relatively low losses in the range of 0.5-5 μm and good chemical stability, hence this material is a very promising candidate for future integrated non-linear photonics. Tellurite glass fibers are increasingly used for high power

#344592 https://doi.org/10.1364/OME.8.003424
Journal © 2018 Received 3 Sep 2018; revised 6 Oct 2018; accepted 8 Oct 2018; published 17 Oct 2018

Optical Materials EXPRESS

supercontinuum generation in the Near and Middle Infra-Red (NIR and MIR) spectral bands due to the high $\chi(3)$ coefficient and relatively low two-photon absorption in these spectral regions [3–5]. Single-mode waveguide structures with a sufficiently large mode area (LMA) based on nonlinear tellurite glass facilitate generation of 15 μJ pulses with spectrum spreading from 0.9 to 2.5 μm [6]. Currently, LMA fibers are the micro-structured fibers with a large number of small holes surrounding the core. Fabrication of micro-structured tellurite LMA fibers with precisely defined core-cladding parameters meets severe technical problems because the viscosity of tellurite glasses strongly depends on temperature compared to silica-based glasses [4–6]. In the soft glass holey fibers, where the hole-radius is small, the surface tension leads to the deformation of microstructures at the fiber drawing temperature [4]. The surface of holes can be contaminated that leads to increase of insertion loss. Single-mode LMA channel waveguide fabricated by direct laser writing in a glass is a promising alternative to micro-structured fiber because it is a single stage process which avoids contamination of fiber core in principle. Such waveguide structures could be more suitable for applications in high power nonlinear integrated optics and compatible to standard single mode fibers.

Currently, a study of laser written waveguides in tellurite glass is in its infant stage [7,8] and there are no studies of their nonlinear optical properties. As far as nonlinear waveguide structures fabricated by direct laser writing in other glasses are concerned, most of the papers are devoted to chalcogenide glasses [9–14]. To the best of our knowledge, only one paper was dealing with prototyping such a device in an oxide glass [15]. In this paper, Yang et al. investigated the inscription of waveguide structures in bismuth borate glass with positive refractive index change, so they had written the waveguide core. Nonlinear property of the waveguide was demonstrated at 1550 nm. A 500 nm spectral broadening by launching of 150 fs pulses was obtained.

In present paper we investigated the nonlinear optical properties of a waveguide written in high purity tellurite glass with an alternative architecture. Since only negative refractive index change can be achieved in the investigated glass composition, a depressed cladding structure was designed and inscribed [8]. Moreover, we consider that laser writing of a cladding comprising numerous parallel tracks of modified material with decreased refractive index allows more flexibility in waveguide design than the multi-scan inscription of a core with a positive refractive index change [8,16–18]. The waveguide core with any predetermined shape should provide efficient coupling with adjacent photonic structures such as circular fibers and planar waveguides. To demonstrate efficiency of the fabricated waveguide, we investigated nonlinear propagation of femtosecond pulses in a single transverse mode. Spectral broadening of up to 158 nm (–10 dB level) in the region of strong positive material and waveguide dispersion was revealed under pumping by 175 fs- pulses at a wavelength of 1030 nm. All the spectrum features originated due to the non-linear propagation were theoretically described and explained by taking into account both the Kerr and the Raman contributions.

## 2. Waveguide inscription

Depressed cladding waveguide was inscribed in the high purity $70TeO_2$-$22WO_3$-$8Bi_2O_3$ glass with low OH content. A beam of a femtosecond laser operating at 1030 nm was focused in the glass sample by Olympus LCPlanN-100x-IR objective lens with NA = 0.85. In our previous investigation, we optimized inscription parameters and waveguide architecture to obtain a single transverse mode waveguide with minimum propagation loss at 1030 nm [8]. Pulse duration, repetition rate, and scan velocity were optimized for writing the smoothest tracks and set to 180 fs, 180 kHz, and 6 mm/s correspondingly. We set the pulse energy to 70 nJ because this value falls to the range, where refractive index change is almost independent on the pulse energy [8]. Thus the chosen pulse energy enables inscription of the most homogeneous identical tracks independently on laser power fluctuations. Refractive index

Optical Materials EXPRESS

change was estimated by QPM method with 10x objective lens at the wavelength of 1065 nm [19]. It was found that the refractive index change is negative with amplitude as high as 0.002.

A 14 mm long waveguide consists of 32 parallel tracks, which form the cladding as shown in Fig. 1. The waveguide ends were ground and polished after inscription. The horizontal spacing $\Delta d$ between the tracks is 1.4 μm. The cross-section of a track is oval in shape and it is elongated in the direction of beam propagation (oval's axes are 0.7 and 25 μm) due to the combined action of the self-focusing and the spherical aberration. The self-focusing is likely manifested in the variation of refractive index in a track along the direction of an inscribing beam (Fig. 1). In such depressed cladding waveguides, the mode leakage has a significant contribution to propagation loss [20]. We attempted to suppress the leakage by increasing the cladding thickness, that is, by adding more tracks on the left and right sides of the core and using the pulse energy that produces elongated tracks providing a thick cladding above and below the core. The set of inscribed tracks surround practically intact almost circular domain of unmodified material which form a circular core with an average diameter of 11 μm.

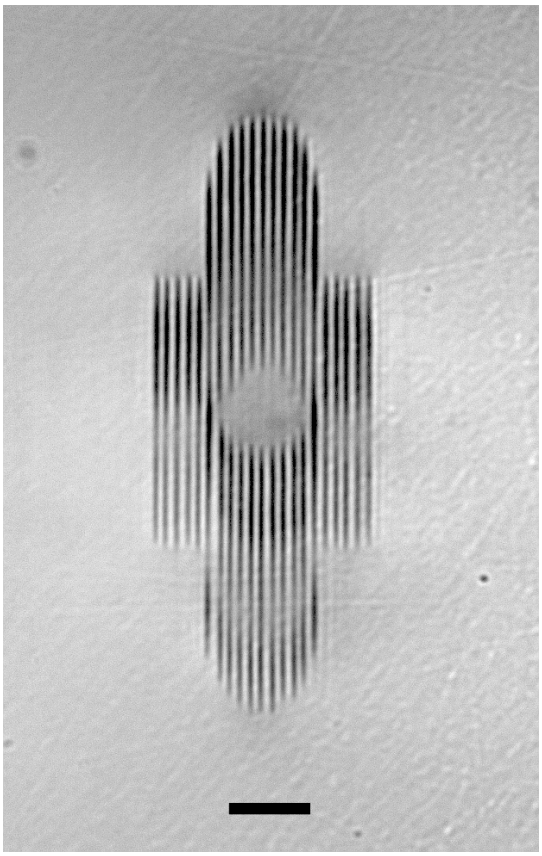

Fig. 1. Bright field microscope picture of the waveguide end. Laser writing beam passed from the top. Scale bar is 10 μm.

## 3. Glass characterization

### *Material absorption*

To estimate material absorption in the wavelength range of 0.75 – 2.7 μm we have drawn a multimode fiber with glass composition investigated and measured insertion loss by the cut-back method. We have got almost uniform absorption, which is only slightly increasing on

Optical Materials EXPRESS

the boundaries of the wavelengths region investigated. The absorption does not exceed 0.02 dB/cm in the whole range of 0.75 – 2.7 μm.

### *Raman gain*

The glass with a chosen composition has the highest nonlinear refractive index among different tellurite glasses investigated before, and its nonlinear coefficient is as high as $5.39 \times 10^{-15}$ cm$^2$/W [8]. This value is 20 times higher than in silica glass.

We have measured the Raman gain spectra of the glass adopting to the method described in [21]. Figure 2 shows the Raman gain spectrum of the investigated glass compared with that of silica glass. It shows that in our tellurite glass Raman gain spectrum has a complex structure consisting of several peaks. The most intense peak at 916 cm$^{-1}$ is 120 times higher than the maximum Raman gain in silica glass (at 450 cm$^{-1}$).

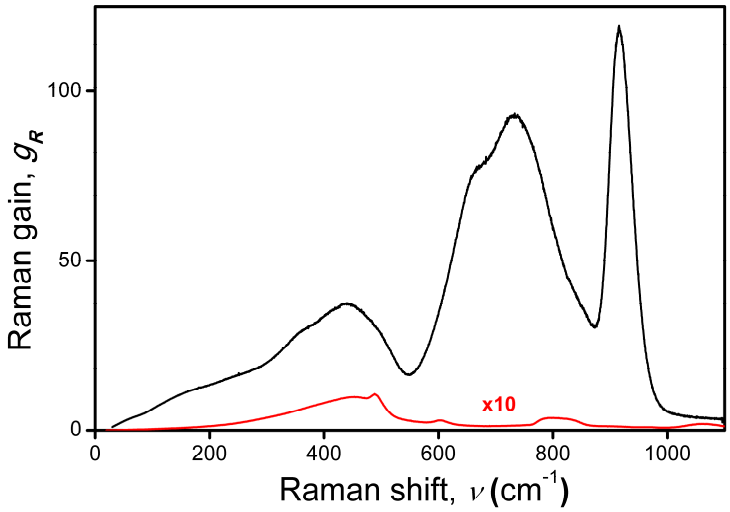


Fig. 2. Raman gain spectra of the $70TeO_2$-$22WO_3$-$8Bi_2O_3$ glass (black solid line) and silica glass (red solid line) for reference (magnified by factor of 10).

### *Dispersion of the refractive index: group velocity dispersion (GVD)*

We have developed an original method for measurement of material dispersion of refractive index, which is an alternative to the well-known interferometric method [22], and is simpler than the latter in optical alignment. A very similar optical scheme that is used in scanning autocorrelators for pulse duration measurement was applied as shown in Fig. 3(a). We determine the first derivative of the propagation constant $\beta_1$, which is the inverse group velocity $u$, from measurements of the femtosecond pulse delay $\Delta t$ in the glass sample:

$$\Delta t = \frac{L}{u} - \frac{L}{c} = \beta_1 L - \frac{L}{c}, \tag{1}$$

where $L$ is the sample length, $c$ is velocity of light in vacuum. Assuming the Sellmeier form for the dispersion of refractive index

$$n(\omega) = \sqrt{1 + \frac{A}{\omega_1^2 - \omega^2} + \frac{B}{\omega_2^2 - \omega^2}}, \tag{2}$$

where $\omega$ is the angular frequency of light, $\beta_1$ can now be determined by the fromula:

Optical Materials EXPRESS

$$\beta_1(\omega) = \left(\frac{\omega n}{c}\right)'_{\omega} = \frac{1 + \frac{A\omega_1^2}{\left(\omega_1^2 - \omega^2\right)^2} + \frac{B\omega_2^2}{\left(\omega_2^2 - \omega^2\right)^2}}{c\sqrt{1 + \frac{A}{\omega_1^2 - \omega^2} + \frac{B}{\omega_2^2 - \omega^2}}}. \quad (3)$$

The pulse delay $\Delta t$ was measured in the wavelength range of 1170-2300 nm for 150-400 fs pulses generated by OPA (Orpheus, Light Conversion), and $\beta_1(\omega)$ was calculated by Eq. (1) accordingly. Then experimental dependence $\beta_1(\omega)$ was approximated by a theoretical one defined by formula (3) while parameters A, B, $\omega_1$, $\omega_2$ were varied (Fig. 3(b)). Thus the dispersion formula for the refractive index of the investigated glass (2) was defined with parameters: A = 420407936 THz$^2$, B = 2398 THz$^2$, $\omega_1$ = 10770 THz, $\omega_2$ = 648 THz. Zero dispersion wavelength (ZDW) was found to be 2120 nm. The close ZDWs differed by less than 100 nm were obtained for the binary tellurite glass [23].

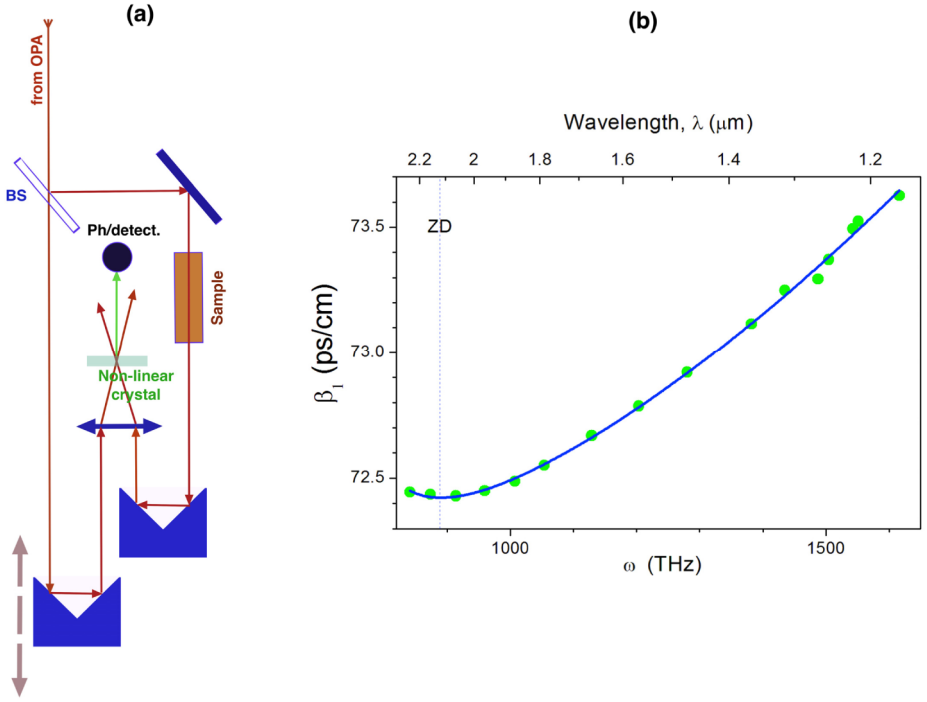


Fig. 3. (a) Optical scheme for measurement of the femtosecond pulse delay in the sample $\Delta t$; (b) Plot of the first derivative of the propagation constant $\beta_1$ against circular frequency $\omega$. Points are the experiment, the solid line is a theoretical fit by formula (3).

## 4. Continuum generation

The nonlinear and waveguide properties of the fabricated structure were studied experimentally with the same femtosecond laser that was used for the waveguide inscription. In these experiments, the laser generated pulses with a duration of 175 fs (FWHM) and a repetition rate of 100 kHz. Figure 4 shows the spectrum of the laser pulses. The spectrum has two peaks structure with multiple shallow peaks.

Optical Materials EXPRESS

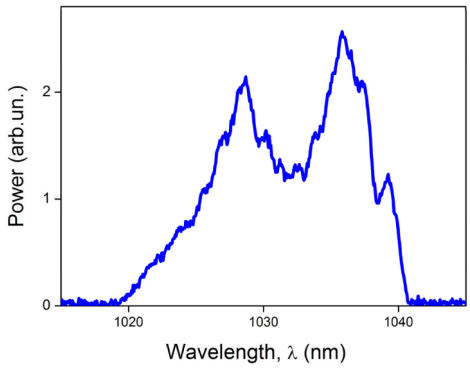


Fig. 4. Spectrum of the 175-fs pulses coupled to the waveguide. Resolution is 0.2 nm.

A polarization attenuator controlled pulse energy $E_{in}$, and a zero-order half-wave plate controlled a direction of linear polarization at the waveguide input. We used an optical system consisting of a plano-concave lens (focal distance is −500 mm) followed by a plano-convex lens (focal distance is 75 mm) for coupling the laser beam with a diameter of 4.5 mm and the $M^2$ factor of 1.2 into the waveguide. Tuning the distance between the lenses allowed careful adjustment of the beam waist diameter to the mode field diameter. The waveguide was set on the 4-axis translation stage. The position of its input end and the distance between the lenses were tuned for maximal coupling of the laser beam under as low input pulse energy as 5 nJ. The output end of the waveguide was imaged on the beam profiler (Spiricon SP620U) with a 10x microscope objective lens.

We found that vertical and horizontal polarizations sustain during propagation through the waveguide. Slightly elliptical Gaussian-like intensity distributions were observed on the beam profiler for both polarizations (Fig. 5). The mode field diameter (MFD) of the fundamental mode at $1/e^2$ intensity level for vertical polarization was measured and found to be 11.0 μm and 13.8 μm for horizontal and vertical cross sections correspondingly. Then the projecting objective lens was removed, and output intensity distribution in the far field, namely, at the distance of 34.5 mm from the output waveguide end, was measured with the same beam profiler. The output beam diameters were found to be 4.81 mm and 4.08 mm, while for an astigmatic Gaussian-like beam with waist diameters equal to MFDs, they should be 4.35 mm and 3.65 mm along the horizontal and the vertical axis correspondingly. Thus the $M^2$ factor of the output beam was found as 1.17 and 1.24 for horizontal and vertical cross sections correspondingly. This result suggests that the waveguide only maintains the transverse fundamental mode.

Optical Materials EXPRESS

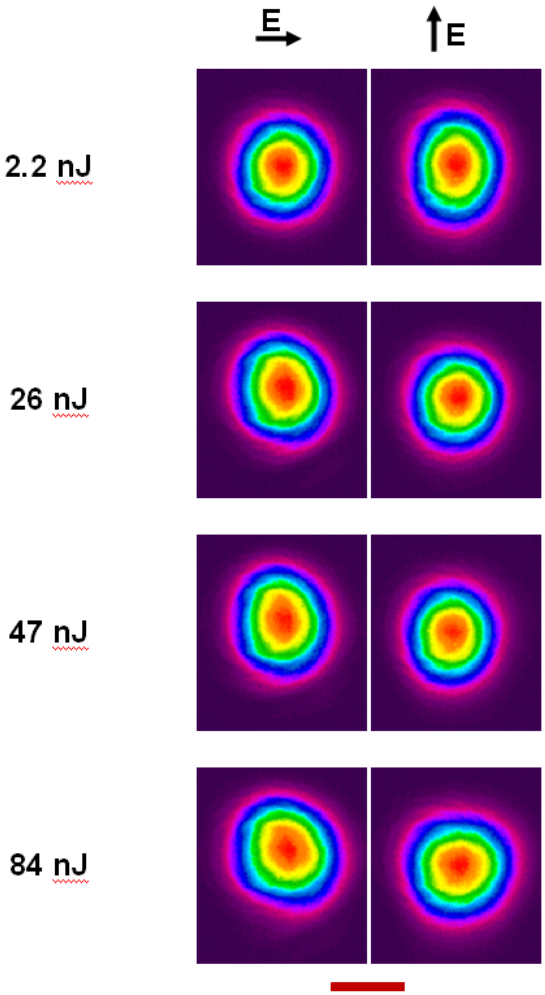


Fig. 5. Intensity distributions at the waveguide output under designated input pulse energies. Arrows show input polarization. Scale bar is 10 μm.

Intensity distributions at the waveguide output at different input pulse energies and polarizations are shown in Fig. 5. These images were taken without any re-alignment of the optical setup, and we only chose a proper neutral density filter for attenuation of the output beam in front of the beam profiler for each input pulse energy. The plot of the MFD versus the input pulse energy is shown in Fig. 6. It demonstrates that the waveguide remains almost single transverse mode for a wide range of input pulse energies and both polarizations. Moreover, MFD is found to be practically independent on both the input pulse energy and the polarization.

Optical Materials EXPRESS

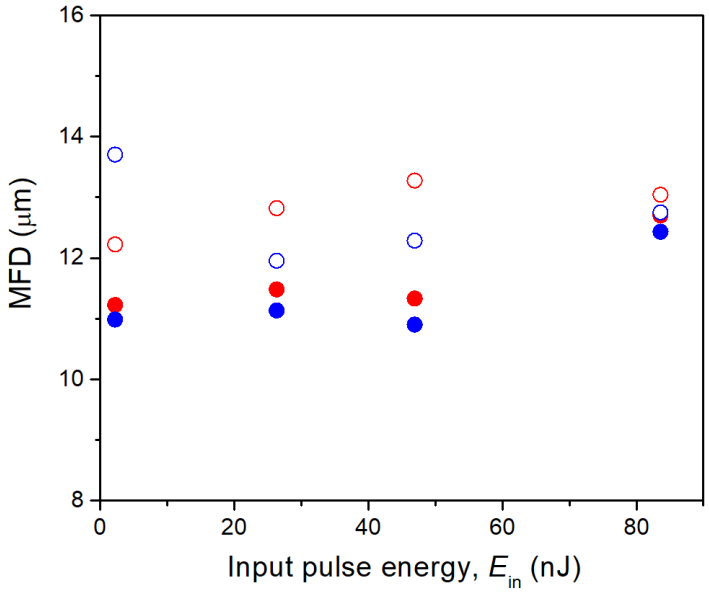


Fig. 6. A plot of MFD against input pulse energy. Red circles are for horizontal polarization, blue circles are for vertical polarization; filled circles are for diameter in the horizontal cross-section, and empty circles are for diameter in the vertical cross-section.

To obtain the waveguide insertion loss, we measured the average laser powers after the 10x objective lens collecting light from the waveguide using the beam profiler with the function "Total power in an aperture". The aperture diameter was set about 3 times larger than the beam diameter. Then the waveguide was removed, and the position of the 10x objective lens was shifted towards the two-lens system so that the laser beam was collimated after the 10x objective lens. Thus we measured the reference power with the same beam profiler and calculated waveguide transmittance. Then upper limit of propagation loss was evaluated taken into account Fresnel reflection at the waveguide input and output. The propagation loss was found to be less than 0.7 dB/cm at 1030 nm for both polarizations.

Spectra of the light emitting from the waveguide were recorded with Yokogawa optical spectrum analyzer with the resolution of 0.2 nm under different input pulse energies in the range of 1- 84 nJ (Fig. 7(a), 7(c), 7(e)). Input pulse energy was kept well below the optical damage threshold on the glass surface that definitely occurred at 400 nJ. However, in the bulk of glass, a much higher threshold of optical damage of up to 5 μJ was observed. The obtained spectra are different to those of input pulses at the pulse energies higher than 3 nJ and typically had more than three peaks. The number of peaks and spectral width monotonously increase with the pulse energy. Forms of the spectra are almost independent on the input polarization. The measured spectra have stochastic nature with characteristic narrow sharp peaks in the central part under all input pulse energies. In Fig. 7(b), 7(d), 7(f) theoretical spectra are shown for comparison, and details of its calculations along with the discussion of unusual spectral shape are given in the next chapter.

Optical Materials EXPRESS

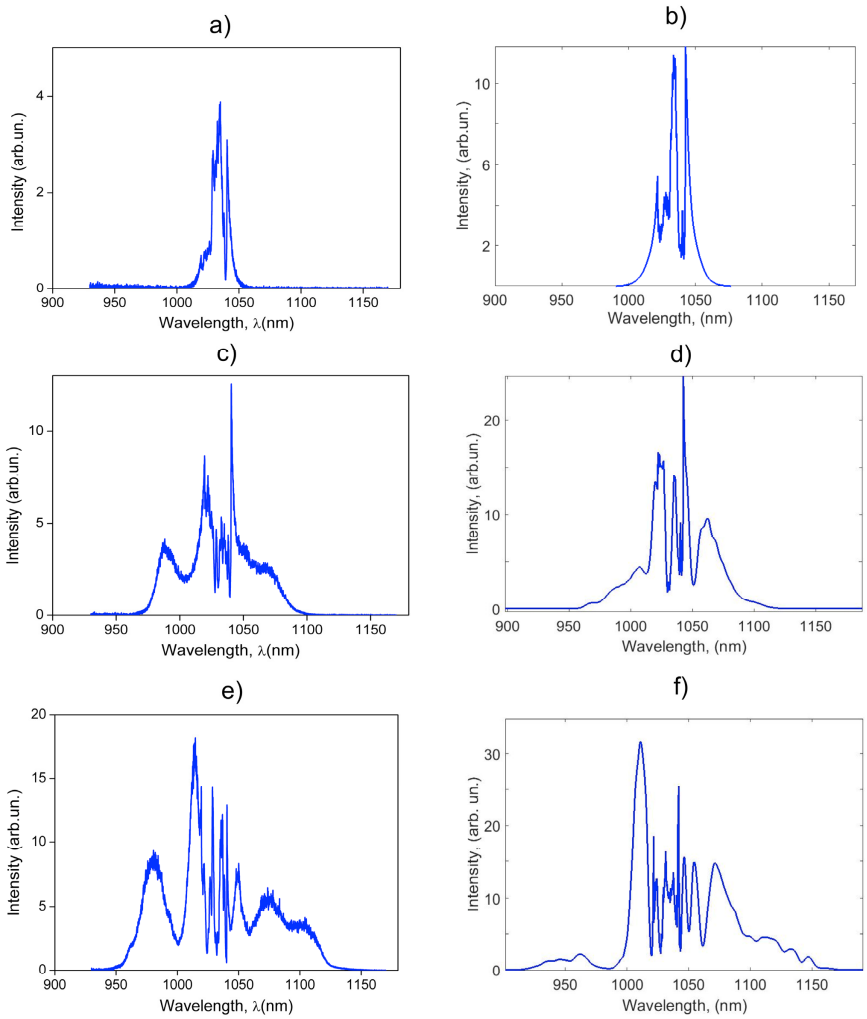


Fig. 7. Spectra of light at the waveguide output obtained experimentally (a), (c), (e) and numerically (b), (d), (f) at input pulse energy $E_{in}$ of 4.7 nJ (a,b), 26 nJ (c,d) and 84 nJ (e,f).

The dependence of the spectral width on the input pulse energy, evaluated at a level of −10 dB relative to the spectral maximum is shown in Fig. 8. It is characterized by the fast growth at low input pulse energies, slowing down while the pulse energy is increasing and saturation at pulse energy around 50 nJ. The maximum spectral width was as high as 158 nm under the input pulse energy of 84 nJ.

Optical Materials EXPRESS

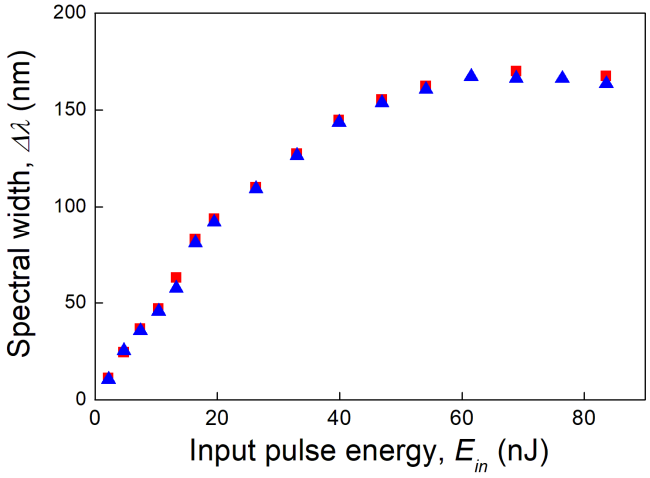


Fig. 8. Plot of measured spectrum widths at the −10 dB level relative spectrum maximum against the input pulse energy. Red points are for horizontal polarization, and blue points are for vertical polarization.

## 5. Numerical analysis of the non-linear propagation and discussions

We used Comsol Multiphysics for the numerical mode analysis. The geometry of the waveguide cross-section used for simulation is shown in the inset of Fig. 9(b). The core size and the parameters of step index tracks (shown in blue color) correspond to experimentally measured values. Refractive index of the glass was calculated according to Sellmeier formula (2). The wavelength dependence of the effective refractive index of the fundamental mode is shown in Fig. 9(a) for horizontal polarization. The dependence of the effective refractive index for the vertical polarization is almost identical. The value of the GVD at the input wavelength of 1030 nm equals 284.9 ps$^2$/km. The wavelength dependence of the confinement loss is shown for the horizontal polarization of the fundamental mode in Fig. 9(b). It should be clarified that for this waveguide, confinement loss gives the main contribution to total loss in the spectral region of 0.75-2.7 μm, since in this spectral region, material loss is below 0.02 dB/cm. The calculated loss of fundamental mode at pump wavelength (0.4 dB/cm) is in agreement with experimentally measured value (0.7 dB/cm). The estimated loss for the first higher mode is more than an order of magnitude higher than for the fundamental mode, which explains a single-mode behavior observed in the experiment.

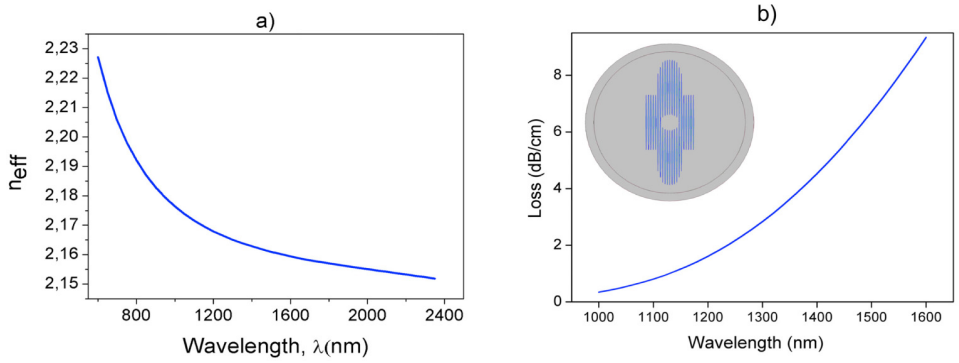


Fig. 9. Calculated wavelength dependence of the effective refractive index (a) and confinement loss of fundamental mode (b). The geometry of the waveguide cross-section along with PML used for calculations is shown in the inset.

Optical Materials EXPRESS

Pulse propagation through the waveguide was investigated numerically using the generalized nonlinear Schrödinger equation (GNSE) for the complex spectral envelope of a pulse, taking into account the higher-order dispersion, the Kerr nonlinearity, and stimulated Raman scattering [24]. The wavelength dependences of the effective mode index, waveguide loss, and effective mode area were also taken into account using the obtained Comsol data for horizontal polarization. The nonlinear response function $R(t) = (1 - f_R)\delta(t) + f_R h_R(t)$ in GNSE includes instantaneous Kerr $\delta(t)$ and Raman $h_R(t)$ contributions to the nonlinear refractive index. Raman nonlinear response function $h_R(t)$ for the glass investigated was calculated from the imaginary part of the third-order susceptibility ( $Im(\chi(3))$ which is proportional to the Raman gain (Fig. 10) [25]. Figure 10 shows the characteristic feature in damped oscillations of the time-domain Raman response at 0.1 ps, which is unique for our tellurite glass composition with high peak at 916 $cm^{-1}$. The similar specific features of the Raman response for other compositions of the tellurite glass were obtained in the paper [26]. The Raman fraction $f_R$, which represents the Raman contribution to the nonlinear refractive index, was evaluated to be 0.49. This value is higher than the value for silica ( $f_R = 0.18$) but is typical for highly nonlinear tellurite glass systems with broad Raman spectrum [26,27].

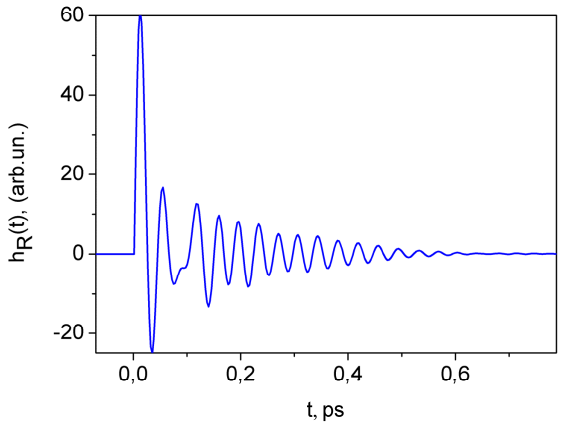


Fig. 10. Raman response function $h_R(t)$ for $70TeO_2$-$22WO_3$-$8Bi_2O_3$ glass.

Numerical analysis was carried out in the Matlab environment using built-in algorithms for performing the fast Fourier transform and solving the nonlinear part of GNSE by the fourth-order Runge – Kutta method with adaptive step. The spectral range from 0.64 to 2.64 μm was divided into $2^{15}$ intervals. The maximum time interval was 92.66 ps.

The dispersion length $L_d = t_0^2/\beta_2$ of 175fs-Gaussian pulses at 1030 nm is 45 mm for the studied waveguide. It exceeds more than threefold the waveguide length. On the other hand, the Kerr nonlinear length $L_{nl} = 1/(\gamma P)$ is 0.2 mm at the input pulse energy of 84 nJ ($P$ = 478 kW), what is about seventy times of magnitude smaller than the waveguide length ($\gamma = (2\pi n_{2Kerr})/(\lambda A_{eff}) = 10^{-4}$ $cm^{-1}W^{-1}$, $n_{2Kerr} = (1-f_R)n_2 = 2.75 \times 10^{-15}$ $cm^2/W$, $\lambda$ = 1030 nm, $A_{eff}$ = 172 $\mu m^2$). Hence the Kerr nonlinearity should play the main role in the evolution of shape and spectrum of the pulse while it propagates through the sample. The characteristic length of Raman gain $L_g = 1/(g_p P)$ is also very small (30 μm) manifesting important role of the Raman scattering in spectrum transformation ($g_p = g_R/A_{eff}$, $g_R = 1.2 \times 10^{-9}$ cm/W, $P$ = 478 kW).

The spectra measured at the waveguide output are characterized by deep modulation structure with characteristic chaotic narrow peaks in the central part, which could not be explained by self-phase modulation of simple Gaussian pulse under a condition that dispersion length $L_d$ is much longer than the nonlinear length $L_{nl}$ [28]. This proposition was

Optical Materials EXPRESS

verified and proved by numerical analysis of the nonlinear propagation a Gaussian pulse without any chirp at the input. However, calculations with the real input pulse spectrum shown in Fig. 4 revealed the spectrum structure in good agreement with the experimental spectra at the same pulse energies (Fig. 7). We consider that pulse with spectrum possessing two maxima could be treated as a superposition of the two coinciding elementary Gaussian pulses with separated spectra and different chirps. Spectra of the elementary pulses are expanding due to self-phase modulation, and so they start to interfere with each other constructively and destructively giving the complicated modulation structure in the spectra. Dependence of the calculated spectral width on the input pulse energy (inset in Fig. 11(a)) is in good agreement with the experimental one (Fig. 8), and confirms saturation of spectrum expansion at a level of –10 dB under input pulse energies exceeding 50 nJ. However, in this energy range growth of spectral broadening continues at the –20 dB level.

We evaluated numerically the prospects of spectrum broadening if the restriction on the input pulse energy imposed by damage on the glass surface is overcome. The input pulse energy was limited to 4 μJ that is slightly lower than the damage threshold in the glass volume (5 μJ). In this case, we obtained a growth of spectrum width up to 600 nm (at –20 dB level), where it saturates (Fig. 11).

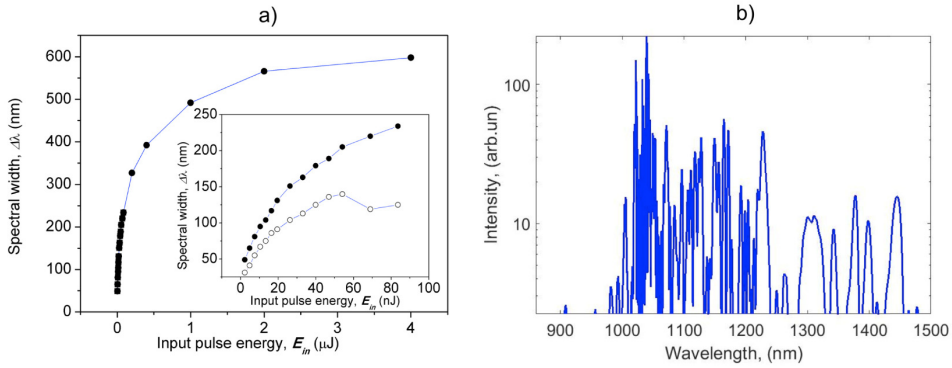


Fig. 11. (a) Spectral width (–20dB level) of the output spectrum versus input pulse power. The initial part of the curve with a relatively fast growth at a level –20 dB (filled circles) is given in a detail in the inset together with the spectral width at a level –10 dB (empty circles); (b) Output spectrum obtained numerically for the input pulse energy of 4 μJ.

The main reason, which prevents obtaining a broader spectrum, is a significant increase of the loss and the effective mode area at wavelengths larger than 1300 nm. Improving waveguide properties is possible through modification of waveguide design. In particular, one should expect the decrease of the loss in the long IR wavelength region for a waveguide with a larger core diameter and increased number of inscribed tracks in a cladding.

It should be noted that our tellurite LMA waveguide has a relatively flat dispersion characteristic with dispersion zero at 2170 nm, which makes it possible to obtain a supercontinuum with a high degree of coherence under pumping by ytterbium femtosecond laser operating in the region of positive dispersion that is far from the dispersion zero.

## 6. Conclusion

The nonlinear optical properties of a large mode area depressed cladding waveguide inscribed in the $70TeO_2$-$22WO_3$-$8Bi_2O_3$ glass were experimentally and numerically studied. Spectrum broadening up to 158 nm (-10 dB level) was obtained in the waveguide when femtosecond pulses with energy of 84 nJ (peak power of 480 kW) at 1030 nm were launched into a 14 mm long waveguide. The waveguide demonstrates single transverse mode propagation with loss lower than 0.7 dB/cm at 1030 nm, the nonlinear coefficient was found to be as high as $10^{-4}$ $cm^{-1}W^{-1}$.

Optical Materials EXPRESS

Raman gain spectrum was measured for the $70TeO_2$-$22WO_3$-$8Bi_2O_3$ glass. The Raman gain extends up to phonons energies of 1000 $cm^{-1}$ with the highest among tellurite glasses maximal value of a Raman gain coefficient equaled to $1.2 \times 10^{-9}$ cm/W at 916 $cm^{-1}$. It is shown that the Raman and Kerr nonlinearities yield almost equal contributions to the nonlinear refractive index.

According to results of numerical calculations, the spectrum broadening could be significantly increased with increasing pump powers. This is possible with improving the polishing of the waveguide ends in order to increase the damage threshold. The spectrum broadening up to 600 nm can be achieved in our 14 mm long sample under input pulse energy of 4 μJ. A significant increase in the loss and effective mode area at wavelengths over 1300 nm is the main reason that prevents to obtain a broader spectrum. A reduction of the propagation loss in the long IR wavelength region is possible in a waveguide with a larger core diameter and increased number of the tracks in a cladding.

## Funding

Russian Science Foundation (RSF) (grant #18-19-00733).

## Acknowledgment

The authors are grateful to G.K. Alagashev, V.V. Likhov, and A.D. Pryamikov for recommendations on methods for calculating the propagation loss in a waveguide.

## References

1. E. Cassan, C. Grillet, D. N. Neshev, and D. J. Moss, "Nonlinear integrated photonics," Photon. Res. **6**(5), NIP1 (2018).
2. S. Gross and M. J. Withford, "Ultrafast-laser-inscribed 3D integrated photonics: Challenges and emerging applications," Nanophotonics **4**(3), 332–352 (2015).
3. P. Domachuk, N. A. Wolchover, M. Cronin-Golomb, A. Wang, A. K. George, C. M. B. Cordeiro, J. C. Knight, and F. G. Omenetto, "Over 4000 nm bandwidth of mid-IR supercontinuum generation in sub-centimeter segments of highly nonlinear tellurite PCFs," Opt. Express **16**(10), 7161–7168 (2008).
4. M. Liao, X. Yan, G. Qin, C. Chaudhari, T. Suzuki, and Y. Ohishi, "A highly non-linear tellurite microstructure fiber with multi-ring holes for supercontinuum generation," Opt. Express **17**(18), 15481–15490 (2009).
5. M. Liao, C. Chaudhari, G. Qin, X. Yan, T. Suzuki, and Y. Ohishi, "Tellurite microstructure fibers with small hexagonal core for supercontinuum generation," Opt. Express **17**(14), 12174–12182 (2009).
6. X. Feng, W. H. Loh, J. C. Flanagan, A. Camerlingo, S. Dasgupta, P. Petropoulos, P. Horak, K. E. Frampton, N. M. White, J. H. Price, H. N. Rutt, and D. J. Richardson, "Single-mode tellurite glass holey fiber with extremely large mode area for infrared nonlinear applications," Opt. Express **16**(18), 13651–13656 (2008).
7. P. Nandi, G. Jose, C. Jayakrishnan, S. Debbarma, K. Chalapathi, K. Alti, A. K. Dharmadhikari, J. A. Dharmadhikari, and D. Mathur, "Femtosecond laser written channel waveguides in tellurite glass," Opt. Express **14**(25), 12145–12150 (2006).
8. M. P. Smayev, V. V. Dorofeev, A. N. Moiseev, and A. G. Okhrimchuk, "Femtosecond laser writing of a depressed cladding single mode channel waveguide in high-purity tellurite glass," J. Non-Cryst. Solids **480**, 100–106 (2018).
9. N. D. Psaila, R. R. Thomson, H. T. Bookey, S. Shen, N. Chiodo, R. Osellame, G. Cerullo, A. Jha, and A. K. Kar, "Supercontinuum generation in an ultrafast laser inscribed chalcogenide glass waveguide," Opt. Express **15**(24), 15776–15781 (2007).
10. M. A. Hughes, W. Yang, and D. W. Hewak, "Spectral broadening in femtosecond laser written waveguides in chalcogenide glass," J. Opt. Soc. Am. B **26**(7), 1370 (2009).
11. J. E. McCarthy, H. T. Bookey, N. D. Psaila, R. R. Thomson, and A. K. Kar, "Mid-infrared guiding and nonlinear spectral broadening in ultrafast laser inscribed gallium lanthanum sulphide waveguides," Opt. Express **20**, 1545 (2012).
12. J. McCarthy, H. Bookey, S. Beecher, R. Lamb, I. Elder, and A. K. Kar, "Spectrally tailored mid-infrared super-continuum generation in a buried waveguide spanning 1750 nm to 5000 nm for atmospheric transmission," Appl. Phys. Lett. **103**(15), 151103 (2013).
13. M. Li, S. Huang, Q. Wang, H. Petek, and K. P. Chen, "Nonlinear lightwave circuits in chalcogenide glasses fabricated by ultrafast laser," Opt. Lett. **39**(3), 693–696 (2014).
14. J. M. Morris, M. D. Mackenzie, C. R. Petersen, G. Demetriou, A. K. Kar, O. Bang, and H. T. Bookey, "$Ge_{22}As_{20}Se_{58}$ glass ultrafast laser inscribed waveguides for mid-IR integrated optics," Opt. Mater. Express **8**(4), 1001 (2018).

Optical Materials EXPRESS


15. W. Yang, C. Corbari, P. G. Kazansky, K. Sakaguchi, and I. C. S. Carvalho, "Low loss photonic components in high index bismuth borate glass by femtosecond laser direct writing," Opt. Express **16**(20), 16215–16226 (2008).
16. F. Chen and J. R. V. de Aldana, "Optical waveguides in crystalline dielectric materials produced by femtosecond-laser micromachining," Laser Photonics Rev. **8**(2), 251–275 (2014).
17. A. G. Okhrimchuk, A. V. Shestakov, I. Khrushchev, and J. Mitchell, "Depressed cladding, buried waveguide laser formed in a YAG:$Nd^{3+}$ crystal by femtosecond laser writing," Opt. Lett. **30**(17), 2248–2250 (2005).
18. D. G. Lancaster, S. Gross, H. Ebendorff-Heidepriem, K. Kuan, T. M. Monro, M. Ams, A. Fuerbach, and M. J. Withford, "Fifty percent internal slope efficiency femtosecond direct-written $Tm^{3+}$:ZBLAN waveguide laser," Opt. Lett. **36**(9), 1587–1589 (2011).
19. C. J. Bellair, C. L. Curl, B. E. Allman, P. J. Harris, A. Roberts, L. M. D. Delbridge, and K. A. Nugent, "Quantitative Phase Amplitude Microscopy IV: imaging thick specimens," J. Microsc. **214**(1), 62–69 (2004).
20. A. Okhrimchuk, V. Mezentsev, and N. Lichkova, "Mid-infrared channel waveguides in RbPb2Cl5 crystal inscribed by femtosecond laser pulses," Opt. Laser Technol. **92**, 80–84 (2017).
21. V. G. Plotnichenko, V. O. Sokolov, V. V. Koltashev, E. M. Dianov, I. A. Grishin, and M. F. Churbanov, "Raman band intensities of tellurite glass," Opt. Lett. **2005**, 1156–1158 (2005).
22. M. Galli, F. Marabelli, and G. Guizzetti, "Direct measurement of refractive-index dispersion of transparent media by white-light interferometry," Appl. Opt. **42**(19), 3910–3914 (2003).
23. G. Ghosh, "Sellmeier Coefficients and Chromatic Dispersions for Some Tellurite Glasses," J. Am. Ceram. Soc. **78**(10), 2828–2830 (1995).
24. J. Dudley and R. Taylor, *Supercontinuum Generation in Optical Fibers* (Cambridge University Press, 2010).
25. R. H. Stolen, J. P. Gordon, W. J. Tomlinson, and H. A. Haus, "Raman response function of silica-core fibers," J. Opt. Soc. Am. B **6**(6), 1159–1166 (1989).
26. X. Yan, G. Qin, M. Liao, T. Suzuki, and Y. Ohishi, "Transient Raman response effects on the soliton self-frequency shift in tellurite microstructured optical fiber," J. Opt. Soc. Am. B **28**(8), 1831–1836 (2011).
27. E. E. Serebryannikov, C. Rivero, R. Stegeman, and A. M. Zheltikov, "Soliton transients and supercontinuum generation in high-Raman-gain materials," J. Opt. Soc. Am. B **24**(1), 137–141 (2007).
28. G. P. Agrawal, *Nonlinear Fiber Optics*, 4th ed. (Academic Press, 2007).